Indian Journal of Pure & Applied Physics
Vol. 58, May 2020, pp. 371-375

Disentangling of incomplete fusion dynamics at low energies ≈ 4-6 MeV/A

Pankaj K Giri[a], Amritraj Mahato[a], D Singh[a*], Sneha B Linda[a], Harish Kumar[b], Suhail A Tali[b], M Afzal Ansari[b], R Kumar[c], S Muralithar[c] & R P Singh[c]

[a]Department of Physics, Central University of Jharkhand, Ranchi 835 205, India

[b]Department of Physics, Aligarh Muslim University, Aligarh 202 002, India

[c]Inter University Accelerator Centre, Aruna Asaf Ali Marg, New Delhi 110 067, India

Received 23 March 2020

An experiment has been performed for the measurements of forward recoil range distributions (FRRDs) of evaporation residues (ERs) using ^{16}O beam on the target ^{148}Nd to explore the incomplete fusion (ICF) dynamics at low projectile energy ≈ 4-6 MeV/A. In the present work, FRRDs of ERs $^{159,158}Er(xn)$, $^{160g,159}Ho(pxn)$, $^{157,155}Dy(\alpha xn)$ and 155Tb(αpxn) have been measured. The measured FRRDs of ERs have been compared with their theoretical mean ranges, calculated using code SRIM. These present results obtained from FRRDs measurements show that full and partial linear momentum transfer components are involved. This indicates that the ERs populated through α-emission channels are not only produced via complete fusion, but also through incomplete fusion dynamics. The present analysis indicates that the incomplete fusion contribution increases with projectile energy. This increment in incomplete fusion contribution is due to the increase in breakup probability of projectile ^{16}O into ^{12}C + ^{4}He/ α with projectile energy.

Keywords: Complete and incomplete fusion, Offline γ-ray spectrometry, Stacked foil activation technique, Excitation functions, Target deformation

1 Introduction

At above the coulomb barrier, complete fusion (CF) and incomplete fusion (ICF) are found to be the dominant reaction modes for the heavy ion (HI) induced reaction at intermediate projectile energy. But the probability of formation of compound nucleus gets slowed down with increasing the projectile energy and ICF starts to dominate over the CF. In case of ICF process, only a part of the projectile fuses with the target while the unfused part moves towards the forward angles as a spectator. Britt and Quinton[1]are the first group to observe this kind of reaction, Galin *et al.*[2] further conformed it. Later on, by utilizing the technique of particle-γ coincidence, Inamura *et al.*[3] brought further advancement in understanding of ICF reactions. Various theoretical models were proposed to explain the complete dynamics of ICF, i.e., the sum rule model by Wilczynski *et al.*[4], break-up fusion model by Udagawa *et al.*[5]. The promptly emitted particle (PEP) model[6], hot spot model[7], multistep direct reaction model[8], etc. are also some of the widely used theoretical models. All these models have been used to reproduce the experimental data at energy above 10 MeV/nucleon. There are many important aspects of ICF reactions at low projectile energy that should be clarified such as; how the ICF dynamics depends on various entrance channel parameters and the angular momenta involved in these reactions. Morgenstern *et al.*[9] reported that, the ICF increases with increasing mass-asymmetry of the system at same relative velocity. Several investigators have made efforts to understand the role of different entrance channel parameters on ICF dynamics[10-12]. Studies show that the ICF dynamics also depends on Coulomb factor ($Z_P Z_T$)[13] and deformation of target (β_2^T)[14,15]. Definite conclusion is yet to be find out regarding the dependence of ICF on various entrance channel parameters or through combined parameters.

The measurement of forward recoil range distributions (FRRDs) is one of the direct method to find out the significant information about the degree of linear momentum transfer (LMT) in heavy ion interaction[16]. This kind of measurements may provide useful information to understand the ICF dynamics. In this paper, the results of FRRDs of various evaporation residues populated through CF and ICF dynamics in the system ^{16}O + ^{148}Nd at beam energy

*Corresponding author (E-mail: dsinghcuj@gmail.com)

range of 4-6 MeV/nucleon are presented. The CF and ICF contribution has also been deduced from the present FRRDs measurements in the studied energy.

2 Experimental Details

The experiments were performed at inter-University Accelerator Centre (IUAC), New Delhi, India. Target irradiations were done at General purpose scattering chamber (GPSC) coupled with in-vacuum transfer facility (IVTF) by utilizing the good quality beam from the 15 UD Pelletron accelerator facilities at the Centre. Stacked foil activation technique has been employed in these measurements. Targets of ^{148}Nd (Enrichment ≈ 98.4%) were prepared by vacuum evaporation technique at target development laboratory of IUAC, New Delhi[17]. In these experiments, 20 thin ^{27}Al-catcher foils of thickness lying in the range ≈ 40-60 μg/cm^2 were used to trap the recoiling ERs. These thin ^{27}Al-catcher foils were prepared by vacuum evaporation technique. The thickness of targets and aluminium catcher foils was determined using α-particle transmission method as well as Rutherford Back Scattering (RBS) technique[17]. The α-particle transmission method is based on the energy loss of 5.485 MeV α-particles emitted from a ^{241}Am source while passing through the ^{148}Nd target and ^{27}Al-catcher foils. Energy Dispersive X-ray Spectroscopy (EDXS)[17] technique was employed to check the purity of targets. The target and ^{27}Al catchers were pasted on rectangular ^{27}Al holders having concentric holes of 1.0 cm diameter. The effective projectile energy is the mid-point energy of the target ^{148}Nd. This energy has been estimated by calculating energy loss of the beam in the ^{148}Nd target using software Stopping and Range of Ions in Matter (SRIM)[18]. The irradiation of these FRRDs stacks were done using $^{16}O^{7+}$-beam of energy ≈ 88, ≈ 92 and ≈ 96 MeV. The stack was irradiated for about 11 hrs due to the half-lives of ERs of interest. The beam current during the irradiation of stack was maintained ~2-3 pnA. The flux of ^{16}O ion beam was determined using a Faraday cup placed at the end of scattering chamber behind the target-catcher foil arrangement. After the irradiation, the activities produced in the irradiated samples were recorded immediately after the irradiation for each target at different time intervals by using 100 c.c. n-type high purity germanium (HPGe) detector connected to a PC through CAMAC based data acquisition system. The software CANDLE[19] was used for the online data recording and offline analysis of the measured data. The energy and efficiency calibration of the HPGe detector was done using the standard ^{152}Eu^g γ-ray source of known strength. A typical calibrated γ-ray spectrum of ^{16}O + ^{148}Nd system at projectile energy ≈88 MeV is shown in Fig. 1. Different γ -ray peaks have been assigned to evaporation residues produced through CF and/or ICF dynamics. The ERs have been identified by observing their characteristic γ-rays and following their half lives in decay curve. Several factors responsible for the uncertainties in the measured cross-sections were discussed in Ref. 14. The overall uncertainty from various factors was estimated to be ≥15%.

3 Results and Discussion

In the present work, FRRDs of ERs ^{159,158}Er(xn), ^{160g,159}Ho(pxn), ^{157,155}Dy(αxn) and ^{155}Tb(αpxn) have been measured measured at three different projectile energies ≈88, ≈92 and ≈96 MeV. Literature data[16, 20] show that the LMT of the different ERs produced via CF and ICF in heavy ion interactions are affected by the projectile energy. In this respect, an attempt has been made to investigate the dependence of LMT of CF and ICF ERs on projectile energy. The disentangling of CF and ICF reaction products have been done in terms of full and partial LMT from projectile ^{16}O to target ^{148}Nd. As a representative case of CF, the measured FRRDs for ER ^{158}Er populated via 6n emission channel from equilibrated compound system ^{164}Er*at the above mentioned three projectile energies are shown in Fig. 2.

As can be seen from these figures, the measured FRRDs show only a single Gaussian peak at each of the above three projectile energies, corresponding to full LMT from projectile ^{16}O to the target ^{148}Nd. Therefore, the ER ^{158}Er is populated via only CF process at each projectile energy. The peaks for the

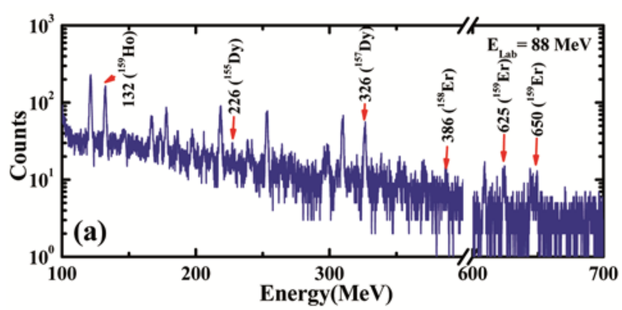

Fig. 1 – Typical γ-ray spectra of induced activity in the Al-catchers recorded in the measurement of FRRDs at cumulative thickness ≈ 509 μg/cm^2 after the interaction of projectile ^{16}O with ^{148}Nd at energy ≈ 88 MeV.

ER ^{158}Er have been found at the cumulative thickness ≈541±19, 561±22 and 604±25 μg/cm^2 respectively for beam energies ≈88, ≈92 and ≈96 MeV. It can also be observed from Fig. 2 that the mean peak position of the CF residue ^{158}Er shifts towards higher cumulative catcher thickness as the projectile energy increases. It is simply because LMT increases with projectile energy. In addition to that, it may be noticed that emission of nucleons from the compound system ^{164}Er* may bring a little change in the energy and momentum of the recoiling nucleus.

On the other hand, as another representative case for α-emission channel, the measured FRRDs for another residue ^{157}Dy populated via α3n emission channel at these three incident energies ≈88, ≈92 and ≈96 MeV are shown in Fig. 3. This figure clearly shows that FRRDs of ER ^{157}Dy have two peaks

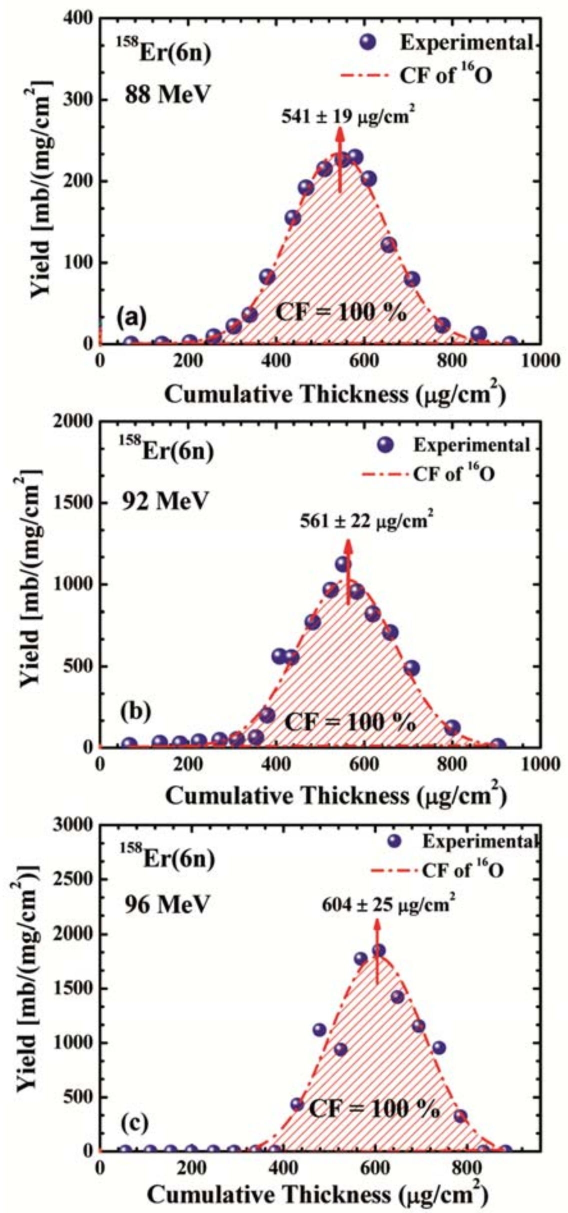

Fig. 2 – Measured FRRDs for the ER ^{158}Er (6n) produced in ^{16}O + ^{148}Nd system at three different projectile energies ≈88, ≈92 and ≈96 MeV, respectively. Solid circles are the experimental data and dashed dot curves represent the Gaussian fit to the measured FRRDs for CF of ^{16}O with ^{148}Nd.

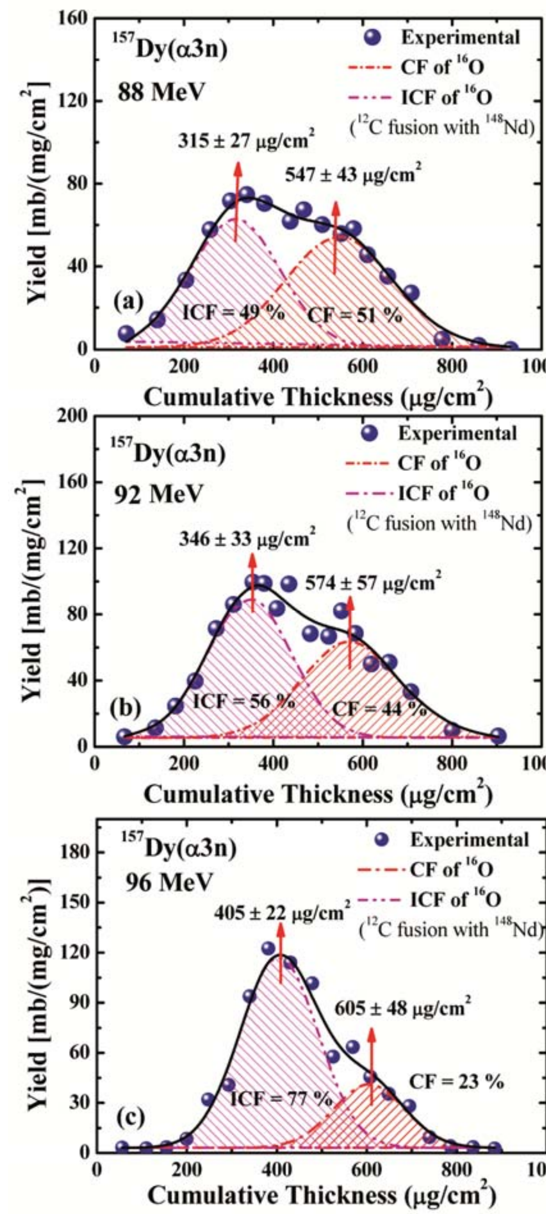

Fig. 3 – Measured FRRDs for the ER ^{157}Dy(α3n) produced in ^{16}O + ^{148}Nd system at three different projectile energies ≈88, ≈92 and ≈96 MeV, respectively. Solid circles are the experimental data and dashed dot curves represent the Gaussian fit to the measured FRRDs for CF of ^{16}O with ^{148}Nd, while dashed dot dot represent the Gaussian fit to the measured FRRDs ICF of ^{16}O (fusion of fragment ^{12}C).

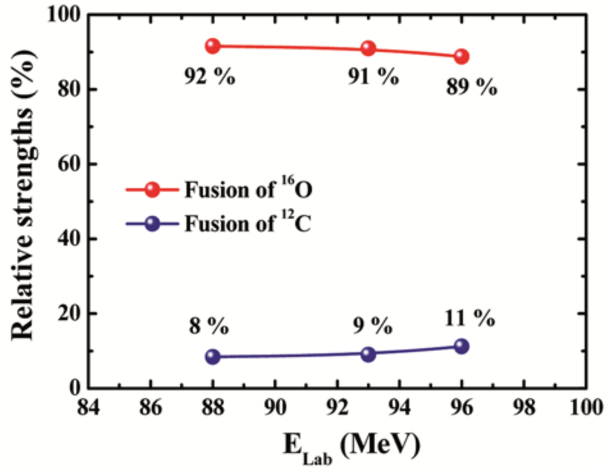

Fig. 4 – Relative strengths of the total contributions from CF and ICF in ^{16}O + ^{148}Nd system at different projectile energies ≈88, ≈92 and ≈96 MeV. The lines joining data points are to guide the eyes.

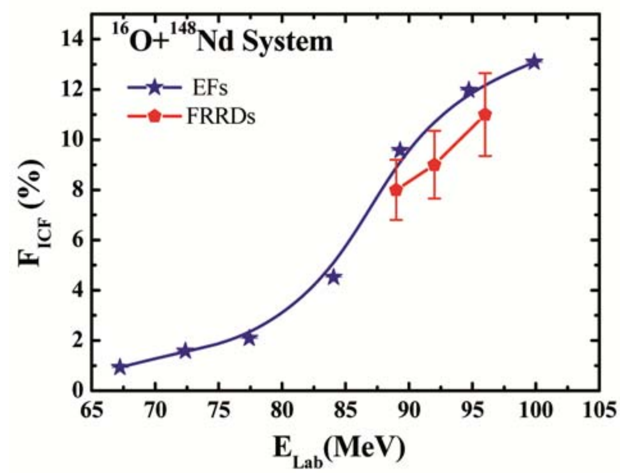

Fig.5 – ICF fraction as a function of projectile energy for the present FRRDs data for the system ^{16}O + ^{148}Nd along with EFs[14] measurements.

structure, one corresponds to full LMT components (i.e., due to the fusion of projectile ^{16}O) and another corresponds to partial LMT components (i.e., due to fusion of fragment ^{12}C with ^{148}Nd). The observed peaks corresponding to full LMT (i.e., in fusion of projectile ^{16}O) were found at cumulative catcher thicknesses ≈547±43, 574±57 and 605±48 μg/cm^2 respectively at three different projectile energies i.e ≈88, ≈92 and ≈96 MeV, while another peaks corresponding to partial LMT transfer (i.e., in fusion of fragment ^{12}C) were found at cumulative Al-catcher foil thicknesses ≈315±27, 346±33 and 405±22 μg/cm^{2}at the same projectile energies as mentioned above. Peaks corresponding to full and partial LMT reveal that this reaction product may be populated via CF and ICF. In these plots, it can be clearly noticed that the position of CF and ICF peaks shifts towards the higher cumulative catcher thickness with increase in incident projectile energy. It was earlier discussed that the mean peaks position of the ER ^{158}Er also shifts towards higher cumulative catcher thickness as the projectile energy increases. This similar behaviour was observed for all ERs produced via CF and ICF in the present system and studied energies.

In order to study the dependency of CF and ICF contribution on projectile energy for the ^{16}O + ^{148}Nd system, the total relative contribution of CF (full LMT) and ICF (partial LMT) components at projectile energies ≈88, ≈92 and ≈96 MeV is also plotted and displayed in Fig. 4. The overall errors in relative contributions are expected to be less than ≈10%. The total relative contributions of CF (fusion of ^{16}O with the target ^{148}Nd) at the projectile energies ≈ 88, ≈92 and ≈ 96 MeV has been found to be ~92%, ~91% and ~89% respectively. On the other hand, the total contributions of ICF (fusion of fragment ^{12}C with the target ^{148}Nd) have been estimated to be ~8%, ~9% and ~11% at these respective energies. It can be noticed from this figure that the relative contribution of ICF significantly increases, while CF contribution decreases with beam energy. These present results suggest that the probability of breakup of ^{16}O projectile (i.e. breakup of ^{16}O in ^{12}C+α) in its interaction with ^{148}Nd increases with projectile energy, while the CF probability decreases with beam energy. Finally, it may be stated that, in general, ICF starts dominating as the projectile energy increases. A plot of ICF fraction as a function of projectile energy for the present FRRDs data along with EFs[14] measurements is shown in Fig. 5. This figure clearly indicates that the ICF fraction rises with projectile energy. It means that the probability of ICF dominates with projectile energy. On the other hand, it has also been noticed that the measured FRRDs data have good consistency with EFs data for same energy regime and system.

4 Conclusions

The forward recoil range distributions (FRRDs) for evaporation residues (ERs)^{159,158}Er(xn), ^{160g,159}Ho(pxn), ^{157,155}Dy(αxn), and, ^{155}Tb(αpxn) populated in the ^{16}O + ^{148}Nd system have been measured at three different projectile energies ≈ 88, ≈92 and ≈96 MeV.The measured FRRDs data have been found to be in support of the excitation function

(EFs) data for the same system ^{16}O + ^{148}Nd system at similar energies. The analysis of measured FRRDs data strongly reveals that there is a significant contribution from the partial linear momentum transfer of the projectile associated with ICF in several α-emitting channels at presently studied energy regime. Different partial linear momentum transfer components may be attributed to the breakup of ^{16}O projectile into ^{12}C and α particle. The FRRDs data also show that the value of LMT for CF and/or ICF components rises with projectile energy. In addition to that, the present results show that probability of breakup of ^{16}O projectile (i.e. breakup of ^{16}O into $^{12}C+\alpha$) in its interaction with ^{148}Nd increases with projectile energy, while the CF probability decreases with beam energy. Finally, the total relative contributions of CF (fusion of ^{16}O with the target ^{148}Nd) at the studied three projectile energies ≈ 88, ≈93 and ≈ 96 MeV has been estimated as ~92%, ~91% and ~89% respectively, while the total contributions of ICF (fusion of fragment ^{12}C with the target ^{148}Nd) has been found to be ~8%, ~9% and ~11% respectively.

Acknowledgement

Authors are grateful to the Director and Convener AUC, IUAC, New Delhi for providing the necessary experimental facilities. Authors are thankful to the target lab in-charge, Mr Abhilash S R and operational staff of pelletron accelerator, IUAC for their support and help during the course of experiment. Authors are expressing their sincere thanks to the Vice-Chancellor and Head, Department of Physics, Central University of Jharkhand, Ranchi for encouragement, motivation and support during the entire work.

References

1 Britt H C & Quinton A R, *Phys Rev*, 124 (1994) 877.
2 Galin J, Gatty B, Guerreau D, Rousset C, Schlotthauer-Voos U C, & Tarrago X, *Phys Rev C*, 9 (1974) 1126.
3 Inamura T, Kojima T, Nomura T, Sugitate T & Utsunomiya H, *Phys Lett B,* 84 (1979) 71.
4 Wilczynski J, Siwek-Wilczynska K, Driel J, Gonggrijp S, Hageman D C J M, Janssens R V F, Łukasiak J & Siemssen R H, *Phys Rev Lett*, 45 (1980) 606.
5 Udagawa T & Tamura T, *Phys Rev Lett*, 45 (1980) 1311.
6 Bondrof J P, De J N, Fai G, Karvinen A O T & Randrup J, *Nucl Phys A*, 333 (1980) 285.
7 Weiner R & Westrom M, *Nucl Phys A*, 286 (1977) 282.
8 Zegrebaev V & Penionzhkevich Y, *Prog Part Nucl Phys*, 35 (1995) 575.
9 Morgenstern H, Bohen W, Galster W, Grabisch K & Kyanowski A, *Phys Rev Lett*, 52 (1984) 1104.
10 Singh D, Giri P K, Mahato A, Linda S B, Kumar H, Ansari M A, Ali R, Tali S A, Rashid M H, Guin R & Das S K, *Nucl Phys A*, 981 (2019) 75.
11 Kumar H, Tali S A, Ansari M A, Singh D, Ali R, Kumar K, Sathik N P M, Parashari S, Ali A, Dubey R, Bala I, Kumar R, Singh R P & Muralithar S, *Nucl Phys A*, 960 (2017) 53.
12 Tali S A, Kumar H, Ansari M A, Ali A, Singh D, Giri P K, Linda S B, Parashari S, Kumar R, Singh R P & Muralithar S, *Nucl Phys A*, 970 (2018) 208.
13 Kumar H, Tali S A, Ansari M A, Singh D, Ali R, Kumar K, Sathik N P M, Ali A, Parashari S, Dubey R, Bala I, Kumar R, Singh R P & Muralithar S, *Eur Phys J A,* 54 (2018) 47.
14 Giri P K, Mahato A, Singh D, Linda S B, Kumar H, Tali S A, Parasari S, Ali A, Ansari M A, Dubey R, Kumar R, Muralithar S & Singh R P, *Phys Rev C*, 100 (2019) 024621.
15 Singh D, Linda S B, Giri P K, Mahato A, Tripathi R, Kumar H, Tali S A, Parashari S, Ali A, Dubey R, Ansari M A, Kumar R, Muralithar S & Singh R P, *Phys Rev C*, 97 (2018) 064610.
16 Singh D, Linda S B, Giri P K, Mahato A, Kumar H, Tali S A, Ansari M A, Kumar R, Muralithar S & Singh R P, *Int J Mod Phys E*, 28 (2019) 1950069.
17 Giri P K, Mahato A, Singh D, Linda S B, Abhilash S R, Deb N K, Umapathy G R, Ojha S, Kabiraj D & Chopra S, *Indian J Pure Appl Phys*, 57 (2019) 675.
18 The Stopping and Range of Ions in Matter (SRIM-2008.04), https://www.srim.org.
19 Kumar B P A, Subramaniam E T & Bhowmik R K, *Conf Proc DAE SNP* (Kolkata, 2001); URL:http:// www.iuac.res.in/NIAS/.
20 Giri P K, Mahato A, Singh D, Linda S B, Kumar H, Tali S A, Ali R, Sathik N P M, Ansari M A, Kumar R, Muralithar S & Singh R P, *Indian J Pure Appl Phys*, 57 (2019) 619.